

Remote Sub-Wavelength Addressing of Quantum Emitters with Chirped Pulses

S. Casulleras,^{1,2} C. Gonzalez-Ballester, ^{1,2} P. Maurer,^{1,2} J. J. Garcia-Ripoll,³ and O. Romero-Isart^{1,2}

¹*Institute for Quantum Optics and Quantum Information of the Austrian Academy of Sciences, 6020 Innsbruck, Austria*

²*Institute for Theoretical Physics, University of Innsbruck, 6020 Innsbruck, Austria.*

³*Instituto de Física Fundamental IFF-CSIC, Calle Serrano 113b 28006 Madrid, Spain.*

We propose to use chirped pulses propagating near a bandgap to remotely address quantum emitters with sub-wavelength resolution. We introduce a particular family of chirped pulses that dynamically self-focus during their evolution in a medium with a quadratic dispersion relation. We analytically describe how the focusing distance and width of the pulse can be tuned through its initial parameters. We show that the interaction of such pulses with a quantum emitter is highly sensitive to its position due to effective Landau-Zener processes induced by the pulse chirping. Our results propose pulse engineering as a powerful control and probing tool in the field of quantum emitters coupled to structured reservoirs.

An exciting platform in quantum optics, both in the microwave [1–8], and the optical [9–19] regime, is obtained by coupling quantum emitters to photonic structures where bandgaps and dispersion relations can be engineered. In essence, these systems allow enhancing and tailoring sub-wavelength light-matter interaction and bath-mediated coupling between quantum emitters. There are multiple applications in the context of quantum simulation [12, 13] and computation [4, 7, 15] as well as in exploring unconventional quantum optics [1–3, 5, 6, 8–11, 14, 16–19]. Most of these setups rely on, or would benefit from, the possibility of electromagnetically addressing individual quantum emitters. However, such addressing can be challenging due to, for instance, insufficient (*e.g.* sub-wavelength) separation between contiguous emitters or to phase mismatch between outside radiation and the electromagnetic modes of the structure. Even in platforms where local probes are available, such as superconducting circuits, these probes might introduce unwanted decoherence and lack the flexibility that a fully tuneable local probe could provide. A potential route towards such individual addressing could be paved by *active* electromagnetic engineering, where not only the dispersion relation but also the time-dependent state of the electromagnetic environment is tailored.

In this paper we explore the possibility of exploiting active engineering in structured electromagnetic reservoirs. In particular, we introduce a specific family of *chirped* electromagnetic pulses and show that, in a medium displaying a quadratic dispersion relation above a bandgap, their free evolution causes them to dynamically self-focus into a single, potentially sub-wavelength, spot. Self-focusing of chirped pulses using materials with nonlinear electromagnetic response (*e.g.* with intrinsic Kerr nonlinearities) have been exploited before [20–22]. In contrast, here we use non-linear dispersion relations that can be engineered with linear lossless materials (*e.g.* photonic crystals). We then study the interaction between these chirped pulses and a quantum emitter, demonstrating the strong impact of the pulse self-focusing on the dynamics of the emitter. Specifically, a quantum emitter situated

at the focusing spot is shown to display radically different dynamics than a quantum emitter situated at any other position. Our results therefore suggest that chirped pulses in structured electromagnetic media can be used to remotely address individual quantum emitters within an array with sub-wavelength separation (see Fig. 1(a) for a schematic representation). While we discuss our results in the context of structured photonic reservoirs, our results can be extended to other implementations where bosonic excitations propagating near a bandgap couple to quantum emitters (*e.g.* phononic networks coupled to color centers in diamond [23]).

More specifically, we consider an electromagnetic medium extended along the z -axis displaying an energy bandgap for electromagnetic modes propagating along z with wavevector $\mathbf{k} = k\mathbf{e}_z$. The bandgap is characterized by a cutoff frequency ω_c , below which there are no z -propagating modes. We consider that for frequencies $\omega \gtrsim \omega_c$ the dispersion relation of the propagating modes can be written as

$$\omega(k) = \omega_c + \frac{v^2}{2\omega_c} k^2. \quad (1)$$

Here v is a dimensional parameter characterizing the band curvature. We assume the z -propagating electromagnetic modes to be tightly confined in the transverse (x, y) plane in order to increase the interaction with quantum emitters, as discussed later. The propagating electromagnetic modes for a given polarization can then be described by a single mode index, namely their longitudinal wavenumber k , and the single band Eq. (1). As mentioned before, the considered electromagnetic medium can be implemented either in the microwave regime or in the optical regime.

In the medium defined above, we focus on the time dynamics of a single component of the electric field as a function of z evaluated at a given position in the transverse plane, say (x_0, y_0) . We label such scalar electric field as $E(z, t) = 2\text{Re}\{E^+(z, t)\}$. As discussed later, $E(z, t)$ is relevant to describe the electric-dipole interaction with a quantum emitter placed at (x_0, y_0, z) . The

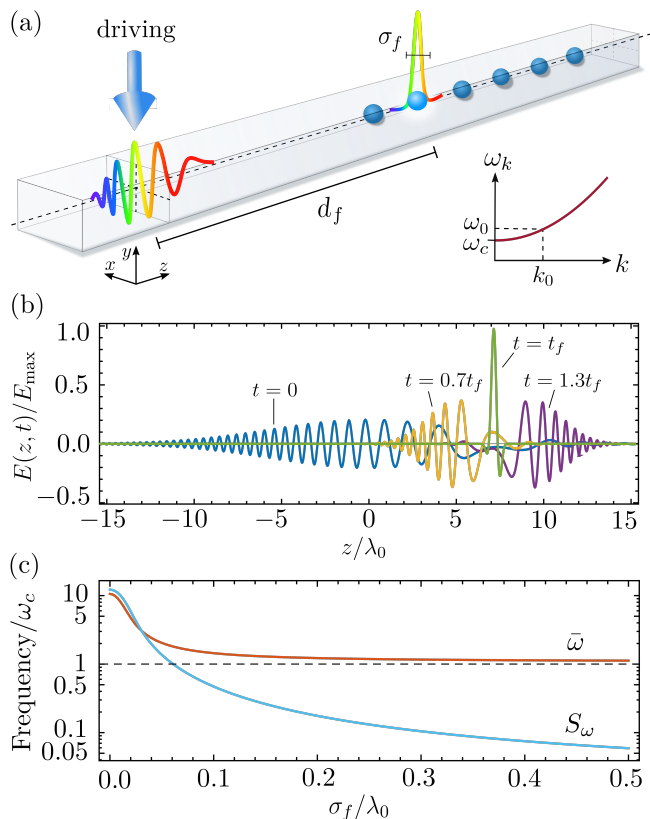


FIG. 1. (a) Quantum emitters embedded in an electromagnetic waveguide. A time-dependent driving applied at the origin of the coordinate system creates a chirped self-focusing electromagnetic pulse. At a time t_f the pulse becomes focused at a distance d_f from the origin, reaching a minimum width σ_f . Inset: Quadratic dispersion relation of the waveguide. The distribution of the pulse wavenumber along z is centered around $k_0 = 2\pi/\lambda_0$. (b) Spatial profile of the electric field of the chirped pulse at different times. The electric field is normalized by its maximum value $E_{\max} = \max_{d,t} E(d,t)$. (c) Mean frequency $\bar{\omega}$ and standard deviation S_ω (defined in the text) of the electric field pulse as a function of the focusing width σ_f . Parameters used: $\omega_0/\omega_c = 1.1$, $d_f/\lambda_0 = 7.5$, $\sigma_f/\lambda_0 = 0.21$, $\phi = 0$.

first main result of this paper is to propose and parameterize a particular family of chirped electromagnetic pulses that dynamically self-focus due to the dispersion relation given by Eq. (1). These pulses depend on five real parameters $(k_0, d_f, \sigma_f, \phi, N)$, defined below, and can be written as

$$E^+(z, t) \equiv |E^+(z, t)| e^{i\theta(z, t)} e^{i\phi} e^{i(k_0 z - \omega_0 t)}. \quad (2)$$

Here k_0 is the carrier wavenumber with corresponding frequency $\omega_0 \equiv \omega(k_0)$ and ϕ is a constant phase. The amplitude of the pulse is given by

$$|E^+(z, t)| \equiv \frac{N}{k_c \sigma(t)} \exp \left[-\frac{\sigma_f^2}{2\sigma^4(t)} \left(z - \frac{vt}{\eta} \right)^2 \right], \quad (3)$$

where $k_c \equiv \omega_c/v$ and $\eta \equiv k_c/k_0$. The time-dependent pulse width is given by

$$\sigma(t) \equiv \sqrt[4]{\sigma_f^4 + \frac{s^2(d_f, t)}{k_c^4}}, \quad (4)$$

where $s(z, t) \equiv \eta k_c z - \omega_c t$ is a spatio-temporal dimensionless function, σ_f is the spot size and d_f the focal distance. The constant N is a pulse amplitude parameter. The time-dependent phase in Eq. (2), which is responsible for the chirping, is given by

$$\theta(z, t) \equiv -\frac{s(d_f, t)s^2(z, t)}{2\eta^2 k_c^4 \sigma^4(t)} + \frac{1}{2} \arctan \left[\frac{s(d_f, t)}{k_c^2 \sigma_f^2} \right]. \quad (5)$$

The pulse $E(z, t)$ is shown in Fig. 1(b) at four particular instants of time, taking $k_0 > 0$ (it propagates rightwards). At $t = 0$ the pulse, centered at $z = 0$, is down-chirped, i.e. the wavelength at the front of the pulse is larger than at its tail. As time increases, free evolution in the quadratic dispersion relation induces self-focusing of the pulse. Specifically, the width $\sigma(t)$ in Eq. (4) becomes smaller following the decrease of the function $s(d_f, t)$. Maximum focusing occurs at a specific time $t_f \equiv \eta d_f/v$, where the width reaches its minimum $\sigma(t_f) = \sigma_f$ and the spatial extension of the pulse is minimized around a focusing point $z = d_f$. At this time, all the components of the pulse sync in phase, namely $\theta(z, t_f) = 0$. At latter times $t > t_f$ the pulse becomes up-chirped and it expands in size. In principle, the focusing distance d_f and width σ_f of the pulse can be arbitrarily chosen, allowing for deep sub-wavelength focusing ($\sigma_f \ll \lambda_0 \equiv 2\pi/k_0$). In Fig. 1(c), we show the mean frequency $\bar{\omega} \equiv \int_{\mathbb{R}} \omega p(\omega) d\omega$ and standard deviation $S_\omega \equiv [\int_{\mathbb{R}} (\omega - \bar{\omega})^2 p(\omega) d\omega]^{1/2}$ of the pulse at $z = 0$ as a function of the focusing width σ_f , using $p(\omega) \equiv |\tilde{E}(0, \omega)| / \int_{\mathbb{R}} |\tilde{E}(0, \omega)| d\omega$ with $\tilde{E}(z, \omega) \equiv (2\pi)^{-1/2} \int_{\mathbb{R}} E(z, t) \exp(-i\omega t) dt$. Stronger focusing (lower σ_f) requires higher mean pulse frequencies and wider distributions in frequency space. We consider hereafter sufficiently large spot sizes, say $\sigma_f \gtrsim 10^{-1} \lambda_0$, such that the spectral properties of the pulse are consistent with the assumptions considered (*e.g.* single band approximation). The frequency distribution of the pulse does not significantly depend on d_f .

One can show that $E(z, t)$, as defined above, is consistent within electrodynamics in the medium Eq. (1). Indeed, $E(z, t)$ has been constructed as a particular linear combination of electromagnetic field modes, engineered in analogy to the wave-packet contracting quantum dynamics of a massive particle evolving in free space, which also displays a quadratic dispersion relation (see the supplemental material in [24]). The chirped electromagnetic pulses can be produced by driving the waveguide at a given spatial position, say at $z = 0$. In [25] we provide a detailed example of how the chirped pulses $E(z, t)$ can be

engineered in a 3D hollow waveguide with perfectly conducting walls [26], a relevant system for circuit quantum electrodynamics [27, 28].

Let us now address the interaction between the self-focusing chirped pulse $E(z, t)$ and a single quantum emitter placed at the position (x_0, y_0, d) . The quantum emitter is first modelled as a qubit with electronic levels $\{|g\rangle, |e\rangle\}$ and transition frequency ω_q . Its electric dipole moment is assumed to point along the direction of the component of the electric field considered in $E(z, t)$. Accordingly, the Hamiltonian describing the electric-dipole interaction of the qubit with the electromagnetic pulse is given by

$$\frac{\hat{H}}{\hbar} = \frac{\omega_q}{2} \hat{\sigma}_z + \frac{\Omega(d, t)}{2} \hat{\sigma}_+ + \frac{\Omega^*(d, t)}{2} \hat{\sigma}_-, \quad (6)$$

where $\Omega(d, t) \equiv -2d_{eg}E(d, t)/\hbar$ is the time- and position dependent Rabi coupling strength, d_{eg} is the dipole matrix element of the qubit and \hbar the reduced Planck constant. We use the Pauli matrix operators for the qubit levels $\hat{\sigma}_z \equiv |e\rangle\langle e| - |g\rangle\langle g|$ and $\hat{\sigma}^\pm \equiv [\hat{\sigma}^\mp]^\dagger = |e\rangle\langle g|$. The dynamics of the state of the qubit $\hat{\rho}(t)$ including spontaneous emission with rate Γ are modeled with the Born-Markov master equation $\partial_t \hat{\rho} = (i\hbar)^{-1} [\hat{H}, \hat{\rho}] + \Gamma(\hat{\sigma}_- \hat{\rho} \hat{\sigma}_+ - [\hat{\sigma}_+ \hat{\sigma}_-, \hat{\rho}]_+)/2$, which can be numerically solved. We remark that the rotating wave approximation, namely using $\Omega(d, t) \equiv -2d_{eg}E^+(d, t)/\hbar$ in Eq. (6), can be employed in the regime $\Omega_0 \ll 2\omega_q$ where $\Omega_0 \equiv \max_{d,t} |\Omega(d, t)|$.

Let us analyze the dynamics of a qubit situated at position $z = d$, and which is initially in the ground state $\hat{\rho}(0) = |g\rangle\langle g|$. Fig. 2(a) shows the excited state probability $p_e(d, t) = \text{tr}[\hat{\rho}(t)|e\rangle\langle e|]$ as a function of time for different positions d of the qubit. When the qubit is situated at the focusing distance ($d = d_f$), the qubit is excited when the pulse reaches it at $t = t_f$ and de-excited when it travels further away. Hence, $p_e(d_f, t \gg t_f) \approx 0$. However, when the qubit is situated far from the focusing distance ($|d - d_f| \gg \sigma_f$), it remains excited at long times $p_e(d \neq d_f, t \gg t_f) \approx 1$. The interaction of the qubit with the pulse happens at a timescale shorter than Γ^{-1} assuming usual spontaneous emission rates $\Gamma/\omega_q \lesssim 10^{-3}$. Fig. 2(b) shows the ground state population of the qubit $p_g(d, t) = \text{tr}[\hat{\rho}(t)|g\rangle\langle g|]$ as a function of the position d of the qubit, at a time τ such that $t_f \ll \tau \ll \Gamma^{-1}$, that is, after the interaction with the pulse but before the decay of the qubit. As shown in [25], Fig. 2(b) does not depend on Γ in the regime $\Gamma/\omega_q \lesssim 10^{-3}$. The plot shows different curves for different values of d_f and σ_f . The ground-state population features a peak of height one centered at the focusing distance of the pulse $d = d_f$ that is narrower the smaller the value of σ_f . The peak manifests that the self-focusing chirped pulse prepares a position-dependent state with a spatial resolution σ_q (the width of the probability peak) that, as further discussed below, is given by $\sigma_q/\sigma_f \approx 1.34$ and thus can be smaller than

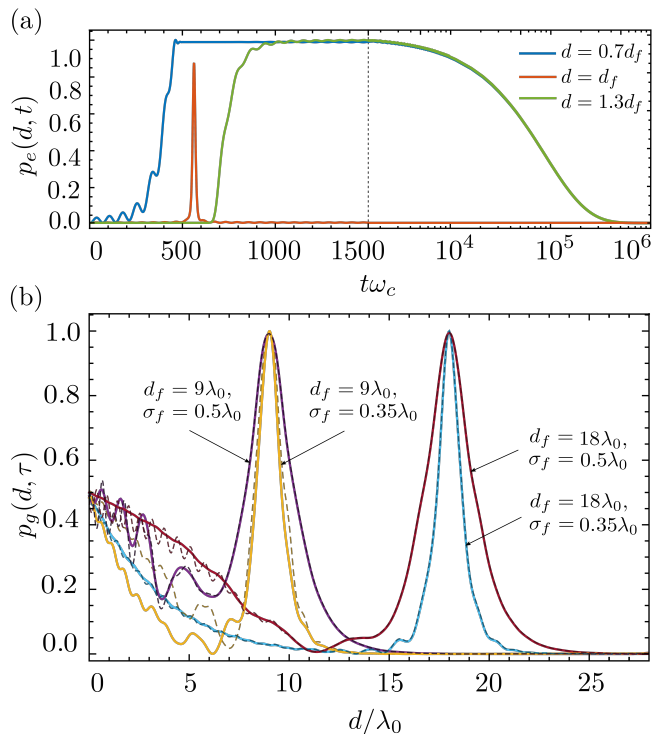


FIG. 2. (a) Excited state population of a qubit of frequency $\omega_q = \omega_0$ as a function of time for different positions of the qubit. We choose $\omega_0/\omega_c = 1.1$, $\Gamma/\omega_0 = 10^{-5}$, $d_f/\lambda_0 = 18$, $\sigma_f/\lambda_0 = 0.35$, $\Omega_0/\omega_c = 0.12$ and $\phi = 0$. (b) Ground state population of the qubit as a function of the on-axis distance d from the origin, for different values of d_f and σ_f (see inset) and at a time τ such that $t_f \ll \tau \ll \Gamma^{-1}$. For this panel we fix $\omega_0/\omega_c = 1.1$ and $\Omega_0/\omega_c = 0.12$ ($\Omega_0/\omega_c = 0.3$) for the curves with $\sigma_f/\lambda_0 = 0.35$ ($\sigma_f/\lambda_0 = 0.5$). Continuous (dashed) lines are calculated with (without) the rotating wave approximation.

$\lambda_q \equiv 2\pi c/\omega_q$. Hence, the proposed self-focusing chirped pulses can be used to perform remote sub-wavelength addressing of quantum emitters with a resolution length scale given by $\sigma_q \propto \sigma_f$.

The dynamics shown in Fig. 2 can be understood in the context of Landau-Zener (LZ) processes [29, 30]. To this end, we consider the Hamiltonian Eq. (6) in the rotating wave approximation and write $\Omega(d, t) \equiv g(d, t) \exp[i\varphi(d, t)]$, where both functions $g(d, t)$ and $\varphi(d, t)$ are real and depend on the amplitude and phase of the electromagnetic pulse, respectively. One then moves to a rotating frame given by the unitary transformation $\hat{U}(t) = \exp[-i\varphi(d, t)\hat{\sigma}_z/2]$, which converts the Hamiltonian (6) into

$$\frac{\hat{H}_{\text{LZ}}}{\hbar} = \Delta(d, t)\hat{\sigma}_z + \frac{g(d, t)}{2}(\hat{\sigma}_+ + \hat{\sigma}_-), \quad (7)$$

where $\Delta(d, t) \equiv \partial_t \varphi(d, t)/2$ for $\omega_q = \omega_0$. In Eq. (7), the qubit detuning $\Delta(d, t)$ (Rabi coupling $g(d, t)$) is time-dependent due to the chirping (time-dependent ampli-

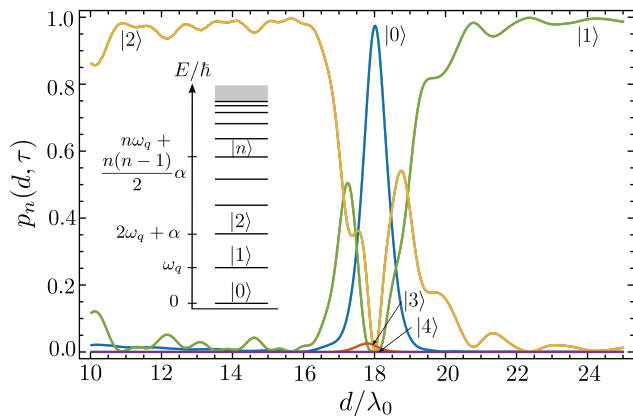


FIG. 3. Population of the internal states of an oscillator with anharmonicity $\alpha/\omega_q = -0.1$ interacting with the pulse as a function of the distance d to the center of the waveguide, at a time τ such that $t_f \ll \tau \ll \Gamma^{-1}$ with $\Gamma/\omega_q = 10^{-5}$. Parameters used: $\omega_q/\omega_c = \omega_0/\omega_c = 1.1$, $d_f/\lambda_0 = 18$, $\sigma_f/\lambda_0 = 0.35$, $\Omega_0/\omega_c = 0.16$, $\phi = 0$.

tude) of the electromagnetic pulse. The results shown in Fig. 2 can be explained in the dressed-state picture of Eq. (7). As further illustrated in [25], within the time interval at which the coupling $g > 0$ and hence an energy gap opens between the dressed energies, the detuning Δ undergoes a single change (two changes) of sign whenever the qubit is out of focus $|d - d_f| \gg \sigma_f$ (on focus $|d - d_f| \ll \sigma_f$). In both regimes the process is adiabatic. Consequently, the out-of-focus qubit goes forth in the lower dressed-energy branch. Hence, after the pulse has passed and the energy gap closes ($g = 0$), the qubit ends up in the excited state. However, in the case when the qubit is on-focus, it goes forth and back in the lower dressed-energy branch, thus ending in the ground state. For distances in the crossover regime $|d - d_f| \approx \sigma_f$ the process includes non-adiabatic transitions as the gap closes while the detuning changes sign. By comparing the timescales at which Δ changes sign and at which the gap opens due to the coupling g , we can estimate and numerically verify that the width of the peak in Fig. 2(b) is given by the above-quoted value of $\sigma_q/\sigma_f \approx 1.34$.

Our results also holds for more complex quantum emitters, such as the nonlinear harmonic oscillator that models a transmon qubit [31]. The Hamiltonian describing the interaction of the quantum emitter with the chirped electromagnetic field pulse is now given by

$$\frac{\hat{H}}{\hbar} = \omega_q \hat{b}^\dagger \hat{b} + \frac{\alpha}{2} \left[(\hat{b}^\dagger \hat{b})^2 - \hat{b}^\dagger \hat{b} \right] + \frac{\Omega(d, t)}{2} \hat{b}^\dagger + \frac{\Omega^*(d, t)}{2} \hat{b}, \quad (8)$$

where \hat{b} (\hat{b}^\dagger) is a bosonic annihilation (creation) operator and $\Omega(d, t) = -2d_q E(d, t)/\hbar$, where d_q is the dipole moment of the anharmonic quantum emitter. One can then numerically solve the Born-Markov master equation $\partial_t \hat{\rho} = (i\hbar)^{-1} [\hat{H}, \hat{\rho}] + \Gamma(\hat{b} \hat{\rho} \hat{b}^\dagger - [\hat{b}^\dagger \hat{b}, \hat{\rho}]_+/2)$ in a truncated sufficiently large Hilbert space. We assume the

initial state is $\hat{\rho}(0) = |0\rangle\langle 0|$, where $\hat{b}^\dagger \hat{b} |n\rangle = n |n\rangle$ with $n = 0, 1, 2, \dots$. In Fig. 3 we plot the excitation probability of the state $|n\rangle$, namely $p_n(t, d) \equiv \langle n | \hat{\rho}(t) | n \rangle$, as a function of d . The population of the ground state features a peak around the focusing position of the pulse, analogously to the two-level quantum emitter. Note that the asymmetry of the electromagnetic pulse before and after the focusing distance is imprinted in the excited state of the anharmonic quantum oscillator.

So far, we have analyzed the interaction of chirped electromagnetic pulses with a single quantum emitter as a function of its position in the waveguide. We expect our results to hold in the case of an ensemble of many quantum emitters, as illustrated in Fig. 1(a), at least in the regime where the number of photons in the electromagnetic pulse is much larger than the number of quantum emitters and the single-photon coupling rate is weak. In this regime, both the interactions between quantum emitters and the backaction of a quantum emitter into the electromagnetic pulse can be neglected. Moreover, for pulses with a moderate photon number, such backaction, which could become relevant, can still be neglected as it acts on a much longer timescale than the dynamics we focus on in this work. The regime of few-photon pulses [32–34] or strongly coupled quantum emitters, which is notably challenging to approach theoretically due to interesting emerging quantum phenomena [35–37] is, in our opinion, a very interesting direction for further research.

The self-focusing behavior described in this work only relies on free propagation in a quadratic dispersion relation, and is thus not specific to the electromagnetic field. An interesting outlook of our work is therefore to explore similar self-focusing dynamics in the wide variety of systems that can display a quadratic spectrum, from condensed matter excitations such as electrons, phonons, and magnons, to collective quasiparticles such as bulk plasmons [38] or exciton-polaritons [39, 40], and even to quantum technological platforms described through tight-binding models, such as cavity arrays [41] and atoms in optical lattices [42]. By providing new probing and controlling capabilities at the quantum level, self-focusing pulses could thus become a relevant asset for quantum technologies in the future.

We acknowledge discussions with M. L. Juan, G. Kirchmair, A. Sharafiev, and M. Zanner. C. G. -B. acknowledges funding from the EU Horizon 2020 program under the Marie Skłodowska-Curie grant agreement no. 796725 (PWAQUTEC). J.J.G.-R. acknowledges support from Project No. PGC2018-094792-B-I00 (MCIU/AEI/FEDER, UE), CAM/FEDER Project No. S2018/TCS-4342 (QUITEMAD-CM) and the Quantum Technology Platform PTI-001 (CSIC).

-
- [1] A. Albrecht, L. Henriët, A. Asenjo-García, P. B. Dieterle, O. Painter, and D. E. Chang, *New J. Phys.* **21**, 025003 (2019).
- [2] N. M. Sundareshan, R. Lundgren, G. Zhu, A. V. Gorshkov, and A. A. Houck, *Phys. Rev. X* **9**, 011021 (2019).
- [3] V. S. Ferreira, J. Banker, A. Sipahigil, M. H. Matheny, A. J. Keller, E. Kim, M. Mirhosseini, and O. Painter, (2020), [arXiv:2001.03240](https://arxiv.org/abs/2001.03240).
- [4] A. Vrajitoarea, Z. Huang, P. Groszkowski, J. Koch, and A. A. Houck, *Nat. Phys.* **16**, 211 (2020).
- [5] I. Carusotto, A. A. Houck, A. J. Kollár, P. Roushan, D. I. Schuster, and J. Simon, *Nat. Phys.* **16**, 268 (2020).
- [6] Y. Schön, J. N. Voss, M. Wildermuth, A. Schneider, S. T. Skacel, M. P. Weides, J. H. Cole, H. Rotzinger, and A. V. Ustinov, *npj Quantum Mater.* **5**, 18 (2020).
- [7] P. Winkel, I. Takmakov, D. Rieger, L. Planat, W. Hasch-Guichard, L. Grünhaupt, N. Maleeva, F. Foroughi, F. Henriques, K. Borisov, J. Ferrero, A. V. Ustinov, W. Wernsdorfer, N. Roch, and I. M. Pop, *Phys. Rev. Applied* **13**, 024015 (2020).
- [8] E. Kim, X. Zhang, V. S. Ferreira, J. Banker, J. K. Iverson, A. Sipahigil, M. Bello, A. González-Tudela, M. Mirhosseini, and O. Painter, (2020), [arXiv:2005.03802](https://arxiv.org/abs/2005.03802).
- [9] P. Lodahl, A. Floris van Driel, I. S. Nikolaev, A. Irman, K. Overgaard, D. Vanmaekelbergh, and W. L. Vos, *Nature* **430**, 654 (2004).
- [10] T. Lund-Hansen, S. Stobbe, B. Julsgaard, H. Thyrestrup, T. Sünner, M. Kamp, A. Forchel, and P. Lodahl, *Phys. Rev. Lett.* **101**, 113903 (2008).
- [11] P. Lodahl, S. Mahmoodian, and S. Stobbe, *Rev. Mod. Phys.* **87**, 347 (2015).
- [12] J. S. Douglas, H. Habibian, C. L. Hung, A. V. Gorshkov, H. J. Kimble, and D. E. Chang, *Nat. Photonics* **9**, 326 (2015).
- [13] A. González-Tudela, C. L. Hung, D. E. Chang, J. I. Cirac, and H. J. Kimble, *Nat. Photonics* **9**, 320 (2015).
- [14] A. González-Tudela, V. Paulisch, D. E. Chang, H. J. Kimble, and J. I. Cirac, *Phys. Rev. Lett.* **115**, 163603 (2015).
- [15] V. Paulisch, H. J. Kimble, and A. González-Tudela, *New J. Phys.* **18**, 043041 (2016).
- [16] J. D. Hood, A. Goban, A. Asenjo-García, M. Lu, S.-P. Yu, D. E. Chang, and H. J. Kimble, *Proc. Natl. Acad. Sci. U.S.A.* **113**, 10507 (2016).
- [17] P. Lodahl, S. Mahmoodian, S. Stobbe, A. Rauschenbeutel, P. Schneeweiss, J. Volz, H. Pichler, and P. Zoller, *Nature* **541**, 473 (2017).
- [18] E. Sánchez-Burillo, D. Zueco, L. Martín-Moreno, and J. J. García-Ripoll, *Phys. Rev. A* **96**, 023831 (2017).
- [19] M. Bello, G. Platero, J. I. Cirac, and A. González-Tudela, *Sci. Adv.* **5** (2019).
- [20] Y. Silberberg, *Opt. Lett.* **15**, 1282 (1990).
- [21] P. Chernev and V. Petrov, *Opt. Lett.* **17**, 172 (1992).
- [22] X. D. Cao, G. P. Agrawal, and C. J. McKinstrie, *Phys. Rev. A* **49**, 4085 (1994).
- [23] M.-A. Lemonde, S. Meesala, A. Sipahigil, M. J. A. Schuetz, M. D. Lukin, M. Loncar, and P. Rabl, *Phys. Rev. Lett.* **120**, 213603 (2018).
- [24] O. Romero-Isart, L. Clemente, C. Navau, A. Sanchez, and J. I. Cirac, *Phys. Rev. Lett.* **109**, 147205 (2012).
- [25] See Supplemental Material for an example of implementation of chirped electromagnetic pulses in a 3D hollow waveguide with perfectly conducting walls and additional figures on the dynamics of an emitter interacting with a chirped pulse, which includes Refs. [24, 26, 43].
- [26] P. Maurer, J. Prat-Camps, J. I. Cirac, T. W. Hänsch, and O. Romero-Isart, *Phys. Rev. Lett.* **119**, 043904 (2017).
- [27] M. Dalmonte, S. I. Mirzaei, P. R. Muppalla, D. Marcos, P. Zoller, and G. Kirchmair, *Phys. Rev. B* **92**, 174507 (2015).
- [28] D. Zoepfl, P. R. Muppalla, C. M. F. Schneider, S. Kasemann, S. Partel, and G. Kirchmair, *AIP Adv.* **7**, 085118 (2017).
- [29] C. Zener and R. H. Fowler, *Proc. R. Soc. A* **137**, 696 (1932).
- [30] N. V. Vitanov and B. M. Garraway, *Phys. Rev. A* **53**, 4288 (1996).
- [31] J. Koch, T. M. Yu, J. Gambetta, A. A. Houck, D. I. Schuster, J. Majer, A. Blais, M. H. Devoret, S. M. Girvin, and R. J. Schoelkopf, *Phys. Rev. A* **76**, 042319 (2007).
- [32] B. Q. Baragiola, R. L. Cook, A. M. Brańczyk, and J. Combes, *Phys. Rev. A* **86**, 013811 (2012).
- [33] A. H. Küllerich and K. Mølmer, *Phys. Rev. Lett.* **123**, 123604 (2019).
- [34] A. H. Küllerich and K. Mølmer, (2020), [arXiv:2003.04573](https://arxiv.org/abs/2003.04573).
- [35] T. Shi, Y. Chang, and J. J. García-Ripoll, *Phys. Rev. Lett.* **120**, 153602 (2018).
- [36] T. Shi, D. E. Chang, and J. I. Cirac, *Phys. Rev. A* **92**, 053834 (2015).
- [37] T. Shi and C. P. Sun, *Phys. Rev. B* **79**, 205111 (2009).
- [38] J. Quinn, *Nucl. Instrum. Methods Phys. Res., B* **96**, 460 (1995).
- [39] J. Kasprzak, M. Richard, S. Kundermann, A. Baas, P. Jeambrun, J. M. J. Keeling, F. M. Marchetti, M. H. Szymańska, R. André, J. L. Staehli, V. Savona, P. B. Littlewood, B. Deveaud, and L. S. Dang, *Nature* **443**, 409 (2006).
- [40] M. Ramezani, A. Halpin, A. I. Fernández-Domínguez, J. Feist, S. R.-K. Rodriguez, F. J. Garcia-Vidal, and J. G. Rivas, *Optica* **4**, 31 (2017).
- [41] M. Hartmann, F. Brandão, and M. Plenio, *Laser Photonics Rev.* **2**, 527 (2008).
- [42] A. W. Glaetzle, K. Ender, D. S. Wild, S. Choi, H. Pichler, M. D. Lukin, and P. Zoller, *Phys. Rev. X* **7**, 031049 (2017).
- [43] W. C. Chew., *Waves and Fields in Inhomogeneous Media* (Wiley-IEEE Press, U.S., 1995).

Supplemental Material

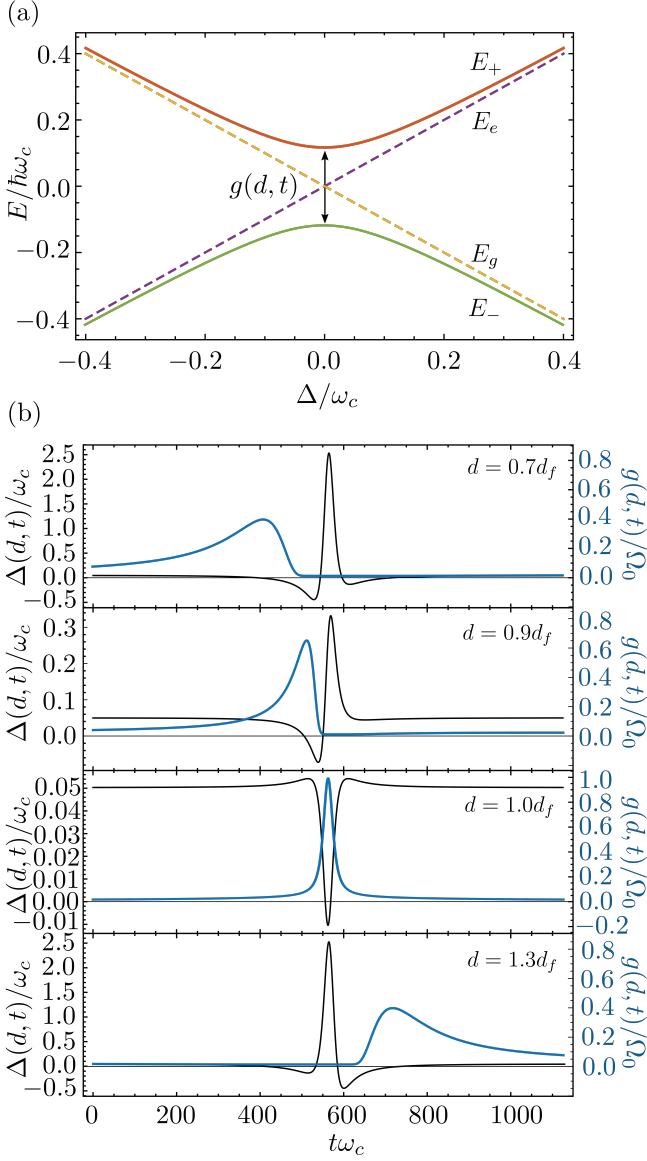


FIG. S1. (a) Energies of the bare (E_g, E_e) and dressed states (E_{\pm}) of the qubit in the Landau-Zener process in Eq. (S15). (b) Detuning (left axis) and coupling strength (right axis) as a function of time for 4 different positions of the qubit (see inset). Parameters used: $\omega_0/\omega_c = 1.1$, $d_f/\lambda_0 = 18$, $\sigma_f/\lambda_0 = 0.35$, $\Omega_0/\omega_c = 0.118$.

EXAMPLE: HOLLOW 3D WAVEGUIDE

Here we describe how to engineer the chirped self-focusing pulse introduced in the main article in a particular setup. We consider a hollow cylindrical waveguide of radius R and infinitely extended along z with perfect electric conducting walls [26]. The following results

are straightforwardly extended to waveguides with other cross-sections.

The electric and magnetic field operators in the waveguide can be expanded in terms of the electromagnetic field modes $\mathbf{f}_{\alpha}(\mathbf{r})$ and eigenfrequencies ω_{α} , where α denotes a multi-index (to be specified below). In particular, we have

$$\hat{\mathbf{E}}(\mathbf{r}) = i \sum_{\alpha} \sqrt{\frac{\hbar\omega_{\alpha}}{2\epsilon_0}} [\mathbf{f}_{\alpha}(\mathbf{r})\hat{a}_{\alpha} - \text{H.c.}], \quad (\text{S1})$$

$$\hat{\mathbf{B}}(\mathbf{r}) = \sum_{\alpha} \sqrt{\frac{\hbar}{2\epsilon_0\omega_{\alpha}}} [\nabla \times \mathbf{f}_{\alpha}(\mathbf{r})\hat{a}_{\alpha} + \text{H.c.}], \quad (\text{S2})$$

where ϵ_0 denotes the vacuum permittivity, \hbar denotes the reduced Planck constant, and \sum_{α} includes the sums (integrals) over discrete (continuous) indices. The creation and annihilation operators, namely $\hat{a}_{\alpha}^{\dagger}$ and \hat{a}_{α} fulfill the commutation relations $[\hat{a}_{\alpha}, \hat{a}_{\alpha'}^{\dagger}] = \delta_{\alpha\alpha'}$ and $[\hat{a}_{\alpha}, \hat{a}_{\alpha'}] = [\hat{a}_{\alpha}^{\dagger}, \hat{a}_{\alpha'}^{\dagger}] = 0$. Here $\delta_{\alpha\alpha'}$ contains a Kronecker (Dirac) delta for each discrete (continuous) index.

The electromagnetic field modes and eigenfrequencies can be determined by solving the eigenmode equation

$$\nabla \times \nabla \times \mathbf{f}_{\alpha}(\mathbf{r}) - \frac{\omega_{\alpha}^2}{c^2} \mathbf{f}_{\alpha}(\mathbf{r}) = 0, \quad (\text{S3})$$

and the boundary condition for perfect electric conducting walls $\mathbf{f}_{\alpha}(\mathbf{r}) \times \mathbf{e}_r = 0$ at $|\mathbf{r}| = R$. Here c denotes the speed of light in vacuum and \mathbf{e}_r denotes the radial unit vector. It can be shown [43] that the electromagnetic field modes split up into two families, namely the transverse electric ($s = \text{TE}$) and the transverse magnetic ($s = \text{TM}$) modes. The electric (magnetic) field of the TE (TM) modes is transverse to the direction of propagation. Furthermore, the modes are denoted by two discrete indices $n \in \mathbb{N}_0$ and $m \in \mathbb{N}$ that characterize the azimuthal and radial distribution of each mode respectively. The continuous index $k \in \mathbb{R}$ denotes the projection of the wavevector on the symmetry axis of the waveguide and completes the multi-index $\alpha \equiv (s, n, m, k)$ which uniquely characterises each mode $\mathbf{f}_{\alpha}(\mathbf{r}) = \mathbf{f}_{nm}^s(k; \mathbf{r})$.

The dispersion relation for the eigenfrequencies is given by

$$\omega_{\alpha} = \omega_{nm}^s(k) \equiv c\sqrt{(k_{nm}^s)^2 + k^2}, \quad (\text{S4})$$

where $k_{nm}^{\text{TM}} \equiv p_{nm}/R$ and $k_{nm}^{\text{TE}} \equiv q_{nm}/R$. The constants p_{nm} and q_{nm} denote the m -th root of the n -th order Bessel function of the first kind $J_n(x)$ and the m -th root of $\partial_x J_n(x)$ respectively. Note that each tuple (s, n, m) , denoted as s_{nm} , characterises an energy band in k . Let us now focus on the lowest TM band, namely TM_{01} . The modes in this band are characterized by a non-zero

electric field component on axis. For modes with $k \ll p_{01}/R$ the dispersion relation can be approximated by the quadratic dispersion relation

$$\omega(k) \equiv \omega_{01}^{\text{TM}}(k) \approx \omega_c + \frac{v^2}{2\omega_c} k^2. \quad (\text{S5})$$

Here $\omega_c \equiv cp_{01}/R$ and $v \equiv c$. Note that higher-order (higher frequency) bands can always be neglected for electromagnetic modes whose frequencies are below the lower cutoff of any such band, namely cp_{nm}/R . Specifically, since the lowest energy band above the TM_{01} band is the TM_{11} band, one can neglect any contribution from higher order bands for modes with frequency $\omega < cp_{11}/R$. Note that the above inequality can always be fulfilled for a sufficiently small radius R .

Let us turn our attention to the corresponding electric field operator. In particular, the expectation value of the z -component of this operator evaluated on the axis of the waveguide is given by

$$\langle \hat{E}_z(z, t) \rangle = i \int_{\mathbb{R}} \sqrt{\frac{\hbar\omega(k)}{2\epsilon_0}} [f_z(k, z) \langle \hat{a}_k(t) \rangle - \text{H.c.}] dk, \quad (\text{S6})$$

where the evolution of the operators $\hat{a}(k) \equiv \hat{a}_{01}^{\text{TM}}(k)$ are given by $\hat{a}(k; t) = \hat{a}(k) \exp[-i\omega(k)t]$. Moreover,

$$f_z(k, z) \equiv \mathbf{f}_{01}^{\text{TM}}(k; z) \cdot \mathbf{e}_z = \frac{iC}{\omega(k)} e^{ikz}, \quad (\text{S7})$$

denotes the z -component of the corresponding field mode along the symmetry axis. Here C is a real constant that depends on the geometry of the waveguide. In particular, for a cylindrical geometry,

$$C = \frac{\omega_c}{R\sqrt{2\pi^2 J_1^2(\omega_c R/c)}}. \quad (\text{S8})$$

Let us assume that the modes of the waveguide are prepared in a coherent state with an amplitude α_k given by

$$\alpha_k = C_\alpha \sqrt{\omega(k)} e^{i\phi} e^{-\frac{\sigma_f^2}{2}(k-k_0)^2} e^{i\frac{d_f}{2k_0}(k-k_0)^2}. \quad (\text{S9})$$

Here C_α is a dimensional constant that can be related to the number of photons in the waveguide, N_{ph} , through

$$N_{\text{ph}} = C_\alpha^2 \sqrt{\pi} \frac{c^2 (2k_0^2 \sigma_f^2 + 1) + 4\sigma_f^2 \omega_c^2}{4\sigma_f^3 \omega_c}. \quad (\text{S10})$$

Evaluating Eq. (S6) with this coherent state leads to the definition of the chirped pulse $E(z, t)$ introduced in the main article. The pulse amplitude N defined in the main text can then be related to C_α through $N = C_\alpha C k_c \sqrt{\pi \hbar / \epsilon_0}$. The particular form of the amplitude $\alpha(k)$ has been chosen in analogy to the wavepacket contracting quantum dynamics of a massive particle evolving in free space, which also follows a quadratic

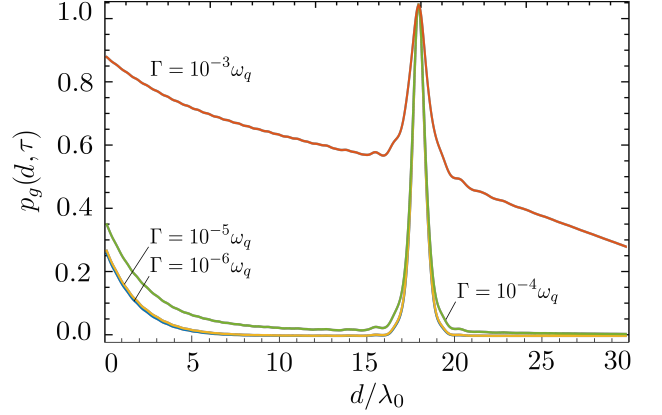


FIG. S2. Ground state population of the qubit after the interaction with the pulse ($\tau/t_f = 3$) as a function of the distance d to the center of the waveguide, for different qubit decay rates Γ . Parameters used: $\omega_q/\omega_c = \omega/\omega_c = 1.1$, $d_f/\lambda_0 = 18$, $\sigma_f/\lambda_0 = 0.35$, $\Omega_0/\lambda_0 = 0.118$.

dispersion relation. In particular, it is equivalent to the momentum representation of the wavepacket that describes a massive particle with an additional initial imaginary phase that causes it to contract (see supplemental material in [24]).

In order to prepare the considered chirped pulse, we must prepare each mode of the waveguide with an amplitude given by the multimode coherent state in Eq. (S9). To this end, we apply a time-dependent driving at a point z_0 along the axis of the waveguide, that we set to $z_0 = 0$. The Hamiltonian of the driven waveguide is in that case

$$\frac{\hat{H}_D}{\hbar} = \int_{\mathbb{R}} \omega(k) \hat{a}^\dagger(k) \hat{a}(k) dk + D(t) \hat{a}(z_0) + D^*(t) \hat{a}^\dagger(z_0), \quad (\text{S11})$$

Here $D(t)$ is a complex function that describes the time-dependent driving. The operators $\hat{a}^\dagger(z_0)$ and $\hat{a}(z_0)$ create or annihilate a photon at the position z_0 , and are related to the operators $\hat{a}(k)$ through

$$\hat{a}(z_0) = \frac{1}{\sqrt{2\pi}} \int_{\mathbb{R}} \hat{a}_k e^{ikz_0} dk. \quad (\text{S12})$$

To obtain the required driving function $D(t)$, we calculate the equations of motion for the expected values $\langle \hat{a}(k) \rangle$ using the Hamiltonian Eq. (S11), and impose that they are equal to the amplitudes in Eq. (S9) after the driving pulse, i.e. at times such that $D(t) = 0$. Under the assumption that the driving function $D(t)$ is extended over a sufficiently long time interval, we obtain a condition for the driving in spectral representation, i.e., for the Fourier transform of the driving function $D(t)$, $\tilde{D}(\omega) \equiv (2\pi)^{-1} \int_{\mathbb{R}} D(t) \exp(-i\omega t) dt$. Specifically, the driving $\tilde{D}(\omega)$ has to fulfill the condition

$$\tilde{D}(\omega(k)) = i\alpha^*(k). \quad (\text{S13})$$

Since $\omega(k)$ is a continuous function with an image in $[\omega_c, \infty)$, this condition fixes the value of the driving for the relevant frequencies $\omega \geq \omega_c$.

Since the Fourier transform of the driving $D(t)$ is proportional to the momentum distribution of the engineered pulse (see Eq. (S13)), it displays similar properties as the ones discussed in Figure 1(c) in the main text, namely it contains components of increasingly high frequency for increasingly focused pulses (i.e. for smaller values of σ_f). Such high frequency components increase the experimental demands required to engineer the driving pulse, ultimately limiting the focusing capabilities. To estimate these limitations, we calculate the electric field profile obtained by removing its high-frequency components above an upper cutoff ω_r , i.e., by setting $\tilde{E}(z, \omega > \omega_r) = 0$, where $\tilde{E}(z, \omega) \equiv (2\pi)^{-1/2} \int_{\mathbb{R}} E(z, t) \exp(-i\omega t) dt$. The cutoff frequency ω_r is determined by the accessible frequencies in the laboratory. The electric field pulse generated by such frequency-truncated spectral distribution is given by

$$E_{\text{truncated}}(z, t) = \frac{1}{\pi} \int_{\mathbb{R}} E(z, s) \frac{\sin[\omega_r(t-s)]}{t-s} ds, \quad (\text{S14})$$

where $E(z, s)$ is the original electromagnetic field pulse (Eq. 2 in the main text). For the range of σ_f and d_f considered in the main article ($d_f/\lambda_0 \gtrsim 10$ and $\sigma_f/\lambda_0 \lesssim 0.5\lambda_0$), one can show that this truncated field remains a good approximation for $E(z, t)$ for upper cutoffs as low as $\omega_r = 2\omega_c$ or, in other words, the electric field profile is not significantly modified after removing its higher frequency components. This suggests that the self-focusing pulses could be realistically engineered in a hollow waveguide, provided that the applied driving approximates well enough the condition in Eq. (S13).

ADDITIONAL FIGURES

Fig. S1(a) shows the instantaneous eigenenergies of the Landau-Zener Hamiltonian

$$\frac{\hat{H}_{\text{LZ}}}{\hbar} = \Delta(d, t) \hat{\sigma}_z + \frac{g(d, t)}{2} (\hat{\sigma}_+ + \hat{\sigma}_-), \quad (\text{S15})$$

as a function of the detuning $\Delta(d, t)$. The energies feature an avoided crossing around $\Delta(t, d) = 0$ with a gap proportional to the coupling strength $g(t, d)$. However, since the coupling strength is time-dependent and only has positive values for a certain time interval, the gap is not always open. When the gap is closed ($g(t, d) = 0$), the eigenstates coincide with the two internal states of the qubit, and their energies are equal to the bare energies (dashed lines in the figure). Fig. S1(b) shows the time dependence of the detuning $\Delta(d, t)$ and the coupling strength $g(d, t)$ due to the interaction between the quantum emitter and the self-focusing pulse, for different positions (x_0, y_0, d) of the emitter. In the figures one can see that the relation between the two relevant timescales, namely the timescale at which the detuning changes sign and the timescale at which the gap opens and closes, depend critically on the qubit position, leading to the dynamics explained in the main article.

Figure S2 shows the ground state population of a qubit placed at the position (x_0, y_0, d) after the interaction with the pulse, for different qubit spontaneous decay rates Γ in the range $\Gamma/\omega_q \in [10^{-6}, 10^{-3}]$. One can see that even for decay rates as large as $\Gamma/\omega_q = 10^{-3}$, there is a significant imprint of the self-focusing pulse on the population of a qubit placed at the focusing point $z = d_f$. The robustness of such imprint against qubit loss stems from the fast qubit-pulse interaction, which happens at much shorter timescales than the dissipation of the qubit.